Arsenic induced autophagy-dependent apoptosis in hippocampal neurons via AMPK/mTOR signaling pathway

Yao Chen
China Medical University
Xudan Liu
China Medical University
Qianhui Zhang
China Medical University
Huanhuan Wang
China Medical University
Ruo Zhang
China Medical University
Yanhong Ge
China Medical University
Huning Liang
China Medical University
Wanying Li
China Medical University
Juanjun Fan
China Medical University
Huimin Liu
China Medical University
Zhengyang Lv
China Medical University
Yi Wang
China Medical University
Xin Li (xli75@cmu.edu.cn)
China Medical University

Research Article

Keywords: Arsenic, PGAM5, autophagy, apoptosis, AMPK, neurotoxicity

Posted Date: February 3rd, 2023

DOI: https://doi.org/10.21203/rs.3.rs-2521006/v1

Abstract

Arsenic contamination of groundwater remains a serious public health problem worldwide. Arsenic-induced neurotoxicity receives increasing attention, however, the mechanism remains unclear. Hippocampal neuronal death is regarded as the main event of arsenic-induced cognitive dysfunction. Mitochondria lesion is closely related to cell death, however, the effects of arsenic on PGAM5-regulated mitochondrial dynamics has not been documented. Crosstalk between autophagy and apoptosis is complicated and autophagy has a dual role in the apoptosis pathways in neuronal cells. In this study, arsenic exposure resulted in mitochondrial PGAM5 activation and subsequent activation of apoptosis and AMPK-mTOR dependent autophagy. Intervention by autophagy activator Rapamycin or inhibitor 3-MA, both targeting at mTOR, accordingly induced activation or inhibition of apoptosis. Intervention by MK-3903 or dorsomorphin, activator or inhibitor of AMPK, received similar results. Our findings suggested that arsenic-induced PGAM5 activation played a role in AMPK-mTOR dependent autophagy and arsenic induced autophagy-dependent apoptosis in hippocampal neurons via AMPK/mTOR signaling pathway.

1. Introduction

Arsenic (As) is a type of metallic element that enters the body mainly through drinking arsenic-rich water, eating crops grown in areas rich in arsenic, and clinical therapeutics such as arsenic-containing drugs that widely used in the treatment for syphilis (arsphenamine), leukemia (arsenic trioxide), and cancer (realgar) (Liu et al. 2018; Nurchi et al. 2020). A number of epidemiological studies have confirmed that arsenic can cross the blood-brain barrier, and chronic arsenic exposure causes damage to the nervous system, which is manifested by decreased capability of language, learning and memory, and intelligence (Bjorklund et al. 2018; Curtis et al. 2018; Kaur et al. 2021). Arsenic-induced cognitive dysfunction were also found in many animal models (Arora et al. 2023; Silva-Adaya et al. 2020; Zhang et al. 2022). However, the underlying mechanism of arsenic-induced neurotoxicity remains unclear. Since arsenic exposure cannot be completely avoided at present, exploring the mechanism of arsenic-induced neurotoxicity is of great significance to provide potential target to protect the health of population under chronic environmental exposure and to correct the medicinal side effects of arsenic.

Hippocampus is one of the most important regions in the central nervous system and plays an important role in the construction of learning and memory in mammals (Sekeres et al. 2018). Hippocampal damage is a major cause of central nervous system disease and cognitive impairment (Sekeres et al. 2021). Adult hippocampal injury causes impairments in working memory, attention, executive function and processing speed (Lange et al. 2019). Therefore, the research on the mechanism of hippocampal neuron injury is of great significance for the prevention and treatment of cognitive impairment diseases.

Neuronal death is the main cause of hippocampal damage. Apoptosis of hippocampal neurons in response to diverse stimuli has been well documented. Recently, autophagy has been reported to be related to apoptosis (D'Arcy 2019). Crosstalk between autophagy and apoptosis has been found in many pathogenesis such as cancer metastasis (Su et al. 2015), liver injury (Wang 2015), and neurological

disease (Liu et al. 2019). However, the crosstalk between autophagy and apoptosis is complicated. It has been reported that autophagy has a dual role in the apoptosis pathways, leading to activation or inhibition of the apoptosis signaling in neuronal cells (Gupta et al. 2021).

Both autophagy and apoptosis are closely related to mitochondrial lesions, while the lesions of mitochondria is one of the key events of arsenic-induced toxicity (Wadgaonkar and Chen 2021). Therefore, the damage of arsenic to nervous system may be related to mitochondrial lesions that trigger autophagy and/or apoptosis signaling, leading to neuronal death. Phosphoglycerate mutase 5 (PGAM5), a key Ser/Thr phosphatase located in mitochondria (Takeda et al. 2009), is involved in regulating multiple processes of mitochondrial homeostasis (Wu et al. 2014) and mediates mitochondrial fission by promoting dynamin-related protein 1 (Drp1) localization in mitochondria (Aspuria and Tamanoi 2004; Ma et al. 2020). However, the effects of arsenic on PGAM5-regulated mitochondrial dynamics has not been documented.

The purpose of this study was to discuss the role of PGAM5 in arsenic-induced mitochondrial dysfunction, the possible interplay between autophagy and apoptosis in neuronal death.

2. Materials And Methods

2.1. Animal experiment

Adult C57BL/6 mice (25–28 g) were purchased from SPF (Beijing) Biotechnology Co., Ltd., China. Mice were kept in a room with a relative humidity of 50–60%, a controlled temperature of 22–25°C, and a light/dark cycle for 12 hours. Mice were randomly divided into 4 groups after one week of adaptive feeding. The 3 experimental groups were exposed to $NaAsO_2$ ($NaAsO_2 \geq 90\%$, Sigma-Aldrich, USA) through drinking water for 12 weeks. $NaAsO_2$ was diluted to the specified concentration including 10 mg/L, 20 mg/L and 40 mg/L by double distilled water. Mice of the control group was provided with double distilled water. Drinking water was freshly prepared twice a week. Recognition index (RI), which reflects the cognitive ability of mice, was assessed by novel object recognition (NOR) test at the end of 12 week and calculated as follow: (RI = New object time / (New object time + Old object time) * 100%). Mice with impaired cognitive ability will show reduced RI due to less exploration of new things. Mice were anesthetized by 1% sodium pentobarbital (50 mg/kg) through intraperitoneal injection and sacrificed. Samples of hippocampus tissues were taken for subsequent experiments. All samples were kept at -80℃ for further analysis. Experimental procedures were carried out in strict accordance with the guidelines of the Ethics Committee of China Medical University with the best efforts to reduce the use of animals and to alleviate animal suffering (KT2022474).

2.2. Cell culture and treatment

The mouse hippocampal neuronal cell line HT-22 was purchased from the Cell Bank of Chinese Academy of Medical Sciences. Cells were cultured in MEM medium (01-052-1ACS, Bioind, Israel). The culture medium was supplemented with 10% fetal bovine serum, 50 U/mL penicillin streptomycin (Invitrogen,

Scotland, United Kingdom), 50 mg/mL, and 1% Non-essential Amino Acid (Cyagen, USA). The cells were cultured at 37°C in an incubator supplied with 5% humidified CO_2. HT-22 cells were treated with different concentrations (0, 4, 6, 8, 10 μM) of $NaAsO_2$ for 24 h and harvested for further study. If intervention was needed, cells were treated with autophagy inhibitor 3-Methyladenine (3-MA, HY-19312, MCE, China, 5 mM, 1h) or activator rapamycin (HY-10219, MCE, China, 2 nM, 1h), AMP-activated protein kinase (AMPK) inhibitor dorsomorphin (HY-13418A, MCE, China, 5 μM, 1h) or activator MK-3903 (HY-107988, MCE, China, 4 nM, 1h) prior to $NaAsO_2$ exposure (10 μM, 24 h).

2.3. Transient transfections

All transfections were performed using Lipofectamine 3000 (RiboBio, China) with 50 nM siRNA oligonucleotides targeting at PGAM5 and the negative siRNA (RiboBio, China). HT-22 cells in logarithmic growth phase were seeded in 6-well plates. Culture medium was discarded after cell attachment. siRNA was transfected in complete medium containing 10% FBS but without antibiotics. The oligonucleotides or the transfection plasmid was added according to the instructions. Cells were then exposed to $NaAsO_2$ at the concentration of 10 μM for 24 h.

2.4. Cell vitality assay

The cell vitality of HT-22 cells was detected by Cell Counting Kit-8 (CCK-8, Absin, China). In brief, HT-22 cells were seeded in 96-well plates at a density of 5×10^3 cells per well. Cells in logarithmic growth phase were treated with $NaAsO_2$ (0–30 μM) for 24 h. 10 μL of CCK-8 solution was added into each well at the culture ending. Cells were then incubated for another 2 h. Finally, the 96-well plates were read at 450 nm by a spectrophotometer (Epoch, BioTek, USA).

2.5. Hematoxylin-Eosin (H&E) staining assay

The hippocampal tissue was fixed in 4% paraformaldehyde for at least 24 h. Tissue blocks were embedded in paraffin and sliced into sections. Paraffin section was deparaffinized by xylene twice and rehydrated using a series of gradient concentration of ethanol and double distilled water. Slides were then stained in Harris hematoxylin solution for 8 min and washed in running tap water for 5 min. Finally, the slides were sealed by neutral gum. The representative images were taken by a fluorescence microscope (Nikon ECLIPSE 80i).

2.6. Transmission electron microscope technique

Fresh hippocampal tissue was collected and put into the electron microscope fixation solution immediately. After fixation, hippocampal tissue was embedded with resin for sectioning. The ultrathin sections were cut into 60–80 nm slices by the ultrathin slicer (Leica UC7, Leica, Germany) and fixed on the 150-mesh copper net with formvar film. After staining and drying, the images were observed under transmission electron microscope (HT7800, Hitachi, Japan) and analyzed.

2.7. Measurement of Malondialdehyde in hippocampus

The hippocampus tissue was grinded by a tissue homogenizer (TissueLyser II, QIAGEN, Germany). Tissue homogenate was centrifuged at 12,000 rpm for 10 min (4℃). The protein concentration was detected by a BCA Protein Quantitation kit (Bio-Rad, CA, USA) according to the direction. Samples were further detected for the level of malondialdehyde (MDA) by a Lipid Peroxidation MDA Assay Kit (A003-1-2, Njjcbio, China).

2.8. Detection of ROS by dichlorodihydrofluorescein diacetate (DCFH-DA) assay

DCFH-DA (Solarbio, China) was used to detect the reactive oxygen species (ROS) production by Flow cytometry (LSRFortessa, BD, USA) or Revolve inverted integrated microscope (PVL-100-G, Echo-labs, USA). HT-22 cells were seeded in the 6-well plates at a density of $1x10^5$ cells/well. After treatment, cells were detected for ROS according to the manufacturer's protocol. ModFit LT or Echo software was used for data collection and analysis.

2.9. Mitochondrial membrane potential detection

Mitochondrial membrane potential △ ψM usually is assessed by the detection of JC-1. When the mitochondrial membrane potential is high, JC-1 accumulates in the mitochondrial matrix in the form of polymer which produce red fluorescence. When the mitochondrial membrane potential is low, JC-1 is in the form of monomer which produce green fluorescence. Briefly, HT-22 cells were cultured in 6-well plates and allowed to grow in logarithmic phase. Cells were then received treatment including $NaAsO_2$ exposure and siRNA intervention, respectively. At the culture ending, cells were treated by JC-1 working solution and incubated for 20 min in the dark. Photoscopic observations were made by revolve inverted integrated microscope (PVL-100-G, Echo-labs, USA).

2.10. ATP content detection

ATP content in arsenic-exposed mice hippocampal tissue and HT-22 cells were detected by an ATP kit (Beyotime, China). The tissue and cells were collected and lysed on ice. The lysis of protein solution was detected for the protein concentration. 100 μl sample was mixed with ATP working solution and incubated at room temperature for 3–5 minutes. Samples were finally detected by a microplate reader (synergy H1, BioTek, USA) at 485 nm.

2.11. Western blot assay

The protein level of *p*-AMPK (1:1000, Cell Signaling), *p*-mTOR (1:1000, Cell Signaling), LC3 (1:1000, Cell Signaling), PGAM5 (1:500, ABClonal), optic atrophy 1 (OPA1, 1:500, Santa Cruz), *p*-DRP1 Ser637 (1:1000, Cell Signaling), *p*-DRP1 Ser616 (1:1000, Cell Signaling), mitofusin 1 (MFN1, 1:500, Proteintech), Bcl-2 (1:500, Santa Cruz), Bax (1:500, Santa Cruz), cleaved-caspase-3 (1:1000, Wanlei) and β-Actin (1:8000, Proteintech) were detected by western blot assay.

RIPA lysis buffer (Beyotime, China, P0013B) containing 1% PMSF (Beyotime, China, ST506) and 1% phosphatase inhibitors (Beyotime, China, P1081) was used to lyse mouse hippocampal tissues and the in vitro cultured cells. Equivalent protein (30 μg per sample) was loaded and separated by SDS-PAGE. Protein bands on the membrane were revealed by an Electrophoresis Gel Imaging Analysis System (BioSpectrum Imaging System, USA). Band intensities were quantified by ImageJ software (NIH, USA).

2.12. Statistical analysis

All data were obtained from at least three independent experiments. Data presented as means ± SD were analyzed by SPSS 22.0 Software (SPSS, Inc., Chicago, IL, USA). Student's independent-samples t-test or one-way ANOVA analysis was applied for statistical analysis depending on the data. The difference was considered to be statistically significant if $P < 0.05$.

3. Results

3.1. Chronic arsenic-exposed mice displayed reduced cognitive ability.

All mice displayed normal activity and mental state during the experiment. No significant differences of body weight, organ coefficient of hippocampus and water intake of mice were found among groups (Fig. 1a). The actual arsenic exposure dose was almost multiplied in a dose-dependent manner (Fig. 1b). The recognition index was dose-dependently reduced (Fig. 1c), indicating decreased cognitive ability of mice under arsenic exposure.

3.2. Mitochondria lesions was found in the hippocampal neurons of chronic arsenic-exposed mice.

Results of H&E staining illustrated damages to the hippocampus, including reduced cell number and abnormal arrangement of neurons in arsenic-exposed mice (Fig. 2a). Results of transmission electron microscopy showed damages to the structure of mitochondria, including incomplete bilayer and abnormal crest morphology, in the hippocampal neuronal cells of arsenic-exposed mice (Fig. 2b). At the same time, the protein level of PGAM5, a mitochondrial phosphatase regulating mitochondrial dynamics, was significantly increased upon arsenic exposure. Meanwhile, the level of its downstream target DRP1, a mitochondrial fission protein, was significantly changed. Phosphorylated DRP1 (Ser616) was significantly up-regulated, however, phosphorylated DRP1 (Ser637) was dramatically down-regulated when compared with those of the control group. Furthermore, the levels of mitochondrial fusion related protein optic atrophy 1 (OPA1) and mitofusin 1 (MFN1) were markedly down-regulated (Fig. 2c). The MDA level of arsenic-exposed mice was dose-dependently increased (Fig. 2d). The ATP level of arsenic-exposed mice was significantly lower than that of the control mice (Fig. 2e). These findings indicated that chronic arsenic exposure resulted in mitochondria lesions in mice hippocampal neurons.

3.3. Chronic arsenic exposure caused apoptosis and AMPK-mTOR dependent autophagy activation in the mice hippocampus.

The energy metabolism-related kinase AMPK, one of the upstream inhibitory regulators of mechanistic target of rapamycin (mTOR), was activated under chronic arsenic exposure. The protein levels of *p*-AMPK in the arsenic-exposed groups were significantly increased in a dose-dependent manner. Meanwhile, as one of the upstream inhibitory regulators of autophagy, the protein level of *p*-mTOR was significantly down-regulated by arsenic exposure. The levels of LC3, the autophagy marker protein, was remarkably up-regulated by arsenic exposure (Fig. 3a). These findings indicated the activation of AMPK-mTOR dependent autophagy in the hippocampus of chronic arsenic-exposed mice.

The apoptosis level of hippocampal cells was also significantly increased under arsenic exposure, which were demonstrated by the significant up-regulation of apoptotic protein Bax and down-regulation of anti-apoptotic protein Bcl-2. The protein level of cleaved-caspase-3 was dose-dependently increased, indicating the activation of apoptosis in hippocampal neurons of chronic arsenic-exposed mice (Fig. 3b).

3.4. Arsenic exposure resulted in mitochondria lesions due to the dynamic disorder regulated by PGAM5 in HT-22 cells.

Based on the results of cell viability assay (Fig. 4a), the stepwise arsenic exposure doses including 0 μM, 2 μM, 4 μM, 6 μM and 10 μM were selected for the subsequent experiments.

Results of western blot analysis showed that the protein level of PGAM5 was significantly activated in a dose-dependent manner. Its downstream target *p*-DRP1 (Ser616) was significantly up-regulated, while *p*-DRP1 (Ser637) was remarkably down-regulated by arsenic administration. Meanwhile, the levels of mitochondrial fusion related proteins MFN1 and OPA1 were significantly decreased after the administration of arsenic when compared with those of the control group (Fig. 4b). Fluorescence staining of JC-1 indicated reduced mitochondrial membrane potential in arsenic-exposed HT-22 cells which were illustrated by gradually increased intensity of green fluorescence and decreased intensity of red fluorescence along with the increase of arsenic exposure dose (Fig. 4c). Results of flow cytometry revealed a dose-dependently increased ROS level in HT-22 cells (Fig. 4d). A similar trend of increased ROS fluorescence intensity in arsenic-exposed HT-22 cells was also observed by dichlorofluorescein staining (Fig. 4e). Moreover, the ATP content was significantly reduced in arsenic-exposed groups compared with that in the control group (Fig. 4f).

These findings suggested that arsenic exposure resulted in mitochondrial lesions mainly manifested by mitochondrial dynamic disorder which subsequently induced ROS generation and ATP depletion.

To further study the role of PGAM5 in arsenic-induced mitochondrial dynamic disorder, siRNA targeting at PGAM5 was used to interfere with its expression in HT-22 cells. The expression of PGAM5 was sharply

knocked down by all the three alternative siRNA oligonucleotides. There was no significant difference in the silencing effect among the three ones. siRNA oligonucleotide 2 was selected in the subsequent experiments (Fig. 5a). Results of western blot showed that the protein levels of PGAM5 and *p*-DRP1 Ser 616 were decreased while *p*-DRP1 Ser 637, OPA1, MFN1 were increased by siPGAM5 treatment (Fig. 5b). At the same time, JC-1 assay showed that interference with PGAM5 expression partially reversed the decline of mitochondrial membrane potential induced by arsenic exposure, which was demonstrated by enhanced red fluorescence intensity but decreased green fluorescence intensity (Fig. 5c). Intervention by siPGAM5 sharply alleviated arsenic-induced ROS generation demonstrated by quantitative detection (Fig. 5d). In addition, intervention by siPGAM5 significantly increased ATP content in arsenic-exposed HT-22 cells (Fig. 5e).

These results suggested that arsenic-induced PGAM5 activation played a role in mitochondrial dynamic disorder in HT-22 cells, leading to subsequent mitochondrial lesions including ROS generation and ATP depletion.

3.5. Arsenic induced activation of apoptosis and AMPK-mTOR dependent autophagy were attenuated by PGAM5 inhibition in HT-22 cells.

The protein levels of *p*-AMPK and LC3 significantly increased in a dose-dependent manner. While the protein level of *p*-mTOR were remarkably decreased upon arsenic stimulation, especially in the groups of 8 μM and 10 μM (Fig. 6a). These findings suggested the activation of AMPK-mTOR dependent autophagy in HT-22 cells.

The protein level of Bcl-2 was dose-dependently decreased. At the same time, the protein levels of Bax and cleaved-caspase-3 were increased upon arsenic stimulation (Fig. 6b). These results indicated the activation of apoptosis in HT-22 cells.

As shown in Fig. 6, intervention by siPGAM5 attenuated arsenic-induced activation of AMPK-mTOR dependent autophagy, which was demonstrated by the significant down-regulation of *p*-AMPK and LC3, and up-regulation of *p*-mTOR (Fig. 6c). Intervention by siPGAM5 diminished arsenic-induced apoptosis simultaneously, which was manifested by remarkably decreased Bax and cleaved-caspase3, and notably increased Bcl-2 (Fig. 6d).

3.6. AMPK-mTOR dependent autophagy was related to apoptosis in arsenic-exposed HT-22 cells.

In order to further study the possible crosslink between autophagy and apoptosis, 3-MA and rapamycin, two regulators of autophagy both targeting at mTOR were used in the subsequent experiments. Rapamycin specially inhibits mTOR and subsequently activates autophagy. 3-MA specifically activates PI3K, the upstream regulator of mTOR, thus activating mTOR and inhibiting autophagy.

Results of western blot showed that rapamycin significantly inhibited *p*-mTOR therefore activated autophagy, which was demonstrated by the significant difference of protein levels between $NaAsO_2$ (-)/rapamycin (-) group and $NaAsO_2$ (-)/rapamycin (+) group (Fig. 7a). Meanwhile, intervention by rapamycin further promoted arsenic-induced autophagy, which was demonstrated by the significant difference of protein levels between $NaAsO_2$ (+)/rapamycin (-) group and $NaAsO_2$ (+)/rapamycin (+) group (Fig. 7a). Similar situation was also found in apoptosis. Intervention by rapamycin further increased arsenic-induced apoptosis in HT-22 cells (Fig. 7b). These findings suggested that autophagy activation simultaneously resulted in apoptosis activation.

On the contrary, 3-MA significantly activated *p*-mTOR therefore inhibited autophagy, which was demonstrated by the significant difference of protein levels between $NaAsO_2$ (-)/3-MA (-) group and $NaAsO_2$ (-)/3-MA (+) group (Fig. 7c). In addition, intervention by 3-MA significantly attenuated arsenic-induced autophagy, which was demonstrated by the significant difference of protein levels between $NaAsO_2$ (+)/3-MA (-) group and $NaAsO_2$ (+)/3-MA (+) group (Fig. 7c). Interestingly, inhibition of autophagy also induced inhibition of apoptosis, which was demonstrated by the significant difference of protein levels between $NaAsO_2$ (-)/3-MA (-) group and $NaAsO_2$ (-)/3-MA (+) group, and between $NaAsO_2$ (+)/3-MA (-) group and $NaAsO_2$ (+)/3-MA (+) group (Fig. 7d). These results indicated that autophagy inhibition simultaneously resulted in apoptosis inhibition.

Since 3-MA and rapamycin both target at mTOR, one of the downstream targets of AMPK. We next used MK-3903 and dorsomorphin, the AMPK activator and inhibitor, to further study the possible link between autophagy and apoptosis.

As shown in Fig. 8, intervention by MK-3903 resulted in significant up-regulation of *p*-AMPK and LC3, and down-regulation of *p*-mTOR (Fig. 8a), indicating the activation of AMPK-mTOR dependent autophagy. Intervention by MK-3903 raised apoptosis simultaneously, which was shown by remarkably increased Bax and cleaved-caspase-3, and notably decreased Bcl-2 (Fig. 8b).

On the contrary, intervention by dorsomorphin induced significant down-regulation of *p*-AMPK and LC3, and up-regulation of *p*-mTOR (Fig. 8c), suggesting the inactivation of AMPK-mTOR dependent autophagy. Simultaneously, intervention by dorsomorphin decreased arsenic-induced apoptosis by down-regulated Bax and cleaved-caspase-3 and up-regulated Bcl-2 (Fig. 8d).

These resulted suggested that AMPK-mTOR dependent autophagy was related to apoptosis in arsenic-exposed HT-22 cells.

4. Discussion

Arsenic affects almost every organ or tissue in the human body and has definite neurotoxic effects, which causes peripheral neuropathy, encephalopathy and neurobehavioral changes (Carlin et al. 2016; Garza-

Lombo et al. 2018). Although the neurotoxicity of arsenic has attracted extensive attention, the exact mechanism remains elusive.

Neuronal cell death is regarded as one of the fundamental events of arsenic-induced neurotoxicity. The activation of neural death pathways in response to arsenic stimulation mainly include intrinsic apoptosis and autophagy-mediated cell death (Garza-Lombo et al. 2019). In the present study, increased intrinsic apoptosis and autophagy were also found in the hippocampus of arsenic-exposed mice with cognitive dysfunction.

As key energy-producing organelles, cellular source of reactive species, and multifaceted regulators of cell death, mitochondria are in charge of controlling cell life and death by a balanced homeostasis regulated principally via fission and fusion (Abate et al. 2020; Bock and Tait 2020). Recent evidence indicates that PGAM5, a mitochondrial Ser/Thr phosphatase, is associated with mitochondrial damage by dephosphorylating Drp1 to promote mitochondrial fission, thus resulting in decreased mitochondrial membrane potential, reduced ATP production and enhanced ROS generation (Dan et al. 2023; Liang et al. 2021). Arsenic is known as a toxicant target on mitochondria and induces oxidative stress (Prakash et al. 2022), however, the role of PGAM5 in arsenic-induced mitochondrial lesions has not been documented before.

Our findings of the present study indicated that arsenic exposure induced mitochondrial damage in hippocampal neurons by activating PGAM5-regulated mitochondrial fission. Knockdown of PGAM5 restored mitochondrial homeostasis which was shown by increased mitochondrial membrane potential and ATP production, and decreased ROS generation. Moreover, AMPK was also found to be activated accompanied by the activation of PGAM5 upon arsenic stimulation. Recent evidence indicates that apart from its conventional roles as an energy switch, AMPK is also a redox sensor and modulator (Wu and Zou 2020). Therefore, the activation of AMPK observed in this study might be the subsequent event induced by less production of ATP and over production of ROS due to the activation of PGAM5-regulated mitochondrial fission.

Activated AMPK regulates cell growth and several other cellular processes including autophagy (Herzig and Shaw 2018). AMPK promotes autophagy directly by phosphorylating its downstream autophagy-related proteins such as mTOR or indirectly by regulating the expression of autophagy-related genes (Li and Chen 2019). In the present study, we found that AMPK activated autophagy in arsenic-exposed hippocampal neurons by phosphorylating mTOR, thus inhibiting its activity.

Abnormal autophagy is associated with many pathological processes of cells and the occurrence of diseases (Klionsky et al. 2021). Increasing evidence suggests that autophagy-mediated death induced by over-activation of autophagy is also an important cause of tissue and organ injury (D'Arcy 2019). Findings from some animal studies have revealed that 3-MA, the autophagy inhibitor, actually has neuroprotective effects (Wen et al. 2008; Xin et al. 2011), indicating the role of autophagy-mediated cell death in neuropathy.

In addition, increasing evidence have pointed out the interaction between autophagy and apoptosis, and some autophagy-related factors involved in apoptosis (D'Arcy 2019). Generally speaking, autophagy precedes apoptosis and maintains the stability of the intracellular environment after stimulation. But once the stress exceeds the intensity threshold, apoptosis or other types of programmed cell death are activated (Gupta et al. 2021; Tschan and Simon 2010). However, the interaction between autophagy and apoptosis is extremely complex. So far, the relationship between autophagy and apoptosis has been controversial. Autophagy may promote cell survival and avoid apoptosis, or eventually lead to cell death, or act together with apoptosis, or exist independently when apoptosis fails (Tschan and Simon 2010). A recent review indicates that autophagy plays a dual role in neuronal cells by activating or inhibiting apoptosis signaling (Gupta et al. 2021).

In the present study, increased autophagy was found accompanied with enhanced apoptosis in response to arsenic exposure in hippocampal neuronal cells. Inhibition of autophagy by 3-MA or promotion of autophagy by rapamycin resulted in decreased apoptosis or increased apoptosis accordingly, suggesting autophagy-dependent apoptosis in arsenic-exposed hippocampal neurons. Similar results were also found by AMPK inhibitor intervention. Since 3-MA and rapamycin both target at mTOR, one of the downstream targets of AMPK, these results suggested the role of AMPK/mTOR pathway in autophagy-dependent apoptosis of arsenic-exposed hippocampal neurons.

However, the role of AMPK/mTOR pathway in apoptosis regulation is controversial. Activation of autophagy by AMPK/mTOR pathway results in both suppression and promotion of apoptosis. For example, activation of AMPK/mTOR played a role in the ameliorative effect of dapagliflozin against experimental colitis through augmenting colonic autophagy and restricting apoptosis (Arab et al. 2021). Copper-induced autophagy through Akt/AMPK/mTOR signaling pathway might potentially generate a protective mechanism for improving copper-induced RAW264.7 cell apoptosis (Luo et al. 2021). On the contrary, some other studies reported apoptosis inhibition due to increased autophagy activated by AMPK/mTOR pathway. For instance, salidroside might reverse apoptosis resistance via the up-regulation of autophagy through AMPKα1-mTOR-ULK1 pathways (Gui et al. 2017). Calycosin showed an inhibitory effect on papillary thyroid cancer via promoting apoptosis and autophagy through AMPK/mTOR pathway (Qu et al. 2022). Similar in our study, we found that arsenic induced autophagy-dependent apoptosis in hippocampal neurons via AMPK/mTOR signaling. Overall, AMPK/mTOR-activated autophagy and the regulatory mechanism of it on apoptosis might be condition-dependent and remains further study.

5. Conclusions

In conclusion, our findings indicated that arsenic activated PGAM5-regulated mitochondrial fission, leading to decreased mitochondrial membrane potential, reduced ATP production, enhanced ROS generation, and subsequently activation of AMPK/mTOR signaling. Arsenic induced autophagy-dependent apoptosis of hippocampal neurons was regulated by AMPK/mTOR pathway.

Declarations

Funding

This work was supported by the National Natural Science Foundation of China (NSFC) [grant number 81872568].

Competing Interests

The authors have no relevant financial or non-financial interests to disclose.

Author Contributions

All authors contributed to the study conception and design. Material preparation was performed by Chen Yao and Zhang Qianhui Data collection and analysis were performed by Chen Yao, Liu Xudan Wang Huanhuan Zhang Ruo. Methodological investigation was performed by Zhang Ruo, Ge Yanhong, Liang Huning, Li Wanying, Liu Huimin. Wang Yi performed conceptualization, supervision and project administration. Li Xin performed conceptualization, supervision, resources, writing-review and editing, project administration, funding acquisition. The first draft of the manuscript was written by Chen Yao and all authors commented on previous versions of the manuscript. All authors read and approved the final manuscript.

Ethical Approval

The research was carried out in strict accordance with the guidelines of the Ethics Committee of China Medical University with the best efforts to reduce the use of animals and to alleviate animal suffering. The Ethical No. KT2022474.

Availability of data and materials

No datasets were used for the research described in the article.

References

1. Abate M, Festa A, Falco M, Lombardi A, Luce A, Grimaldi A, et al., 2020. Mitochondria as playmakers of apoptosis, autophagy and senescence. Semin Cell Dev Biol 98, 139-153. https://doi.org/10.1016/j.semcdb.2019.05.022.
2. Arab HH, Al-Shorbagy MY, Saad MA, 2021. Activation of autophagy and suppression of apoptosis by dapagliflozin attenuates experimental inflammatory bowel disease in rats: Targeting AMPK/mTOR, HMGB1/RAGE and Nrf2/HO-1 pathways. Chem Biol Interact 335, 109368. https://doi.org/10.1016/j.cbi.2021.109368.
3. Arora MK, Singh D, Tomar R, Jangra A, 2023. Neuroprotective Efficacy of Edaravone against Arsenic-Induced Behavioral and Neurochemical Deficits in Rats: Amelioration of Cholinergic and

Mitochondrial Functions. CNS Neurol Disord Drug Targets 22, 125-136. https://doi.org/10.2174/1871527321666220225112241.

4. Aspuria PJ, Tamanoi F, 2004. The Rheb family of GTP-binding proteins. Cell Signal 16, 1105-12. https://doi.org/10.1016/j.cellsig.2004.03.019.
5. Bjorklund G, Aaseth J, Chirumbolo S, Urbina MA, Uddin R, 2018. Effects of arsenic toxicity beyond epigenetic modifications. Environ Geochem Health 40, 955-965. https://doi.org/10.1007/s10653-017-9967-9.
6. Bock FJ, Tait S, 2020. Mitochondria as multifaceted regulators of cell death. Nat Rev Mol Cell Biol 21, 85-100. https://doi.org/10.1038/s41580-019-0173-8.
7. Carlin DJ, Naujokas MF, Bradham KD, Cowden J, Heacock M, Henry HF, et al., 2016. Arsenic and Environmental Health: State of the Science and Future Research Opportunities. Environ Health Perspect 124, 890-9. https://doi.org/10.1289/ehp.1510209.
8. Curtis TM, Hannett JM, Harman RM, Puoplo NA, Van de Walle GR, 2018. The secretome of adipose-derived mesenchymal stem cells protects SH-SY5Y cells from arsenic-induced toxicity, independent of a neuron-like differentiation mechanism. Neurotoxicology 67, 54-64. https://doi.org/10.1016/j.neuro.2018.04.009.
9. Dan S, Duan X, Yu X, Zang J, Liu L, Wu G, 2023. PGAM5 regulates DRP1-mediated mitochondrial fission/mitophagy flux in lipid overload-induced renal tubular epithelial cell necroptosis. Toxicol Lett 372, 14-24. https://doi.org/10.1016/j.toxlet.2022.10.003.
10. D'Arcy MS, 2019. Cell death: a review of the major forms of apoptosis, necrosis and autophagy. Cell Biol Int 43, 582-592. https://doi.org/10.1002/cbin.11137.
11. Garza-Lombo C, Pappa A, Panayiotidis MI, Gonsebatt ME, Franco R, 2019. Arsenic-induced neurotoxicity: a mechanistic appraisal. J Biol Inorg Chem 24, 1305-1316. https://doi.org/10.1007/s00775-019-01740-8.
12. Garza-Lombo C, Posadas Y, Quintanar L, Gonsebatt ME, Franco R, 2018. Neurotoxicity Linked to Dysfunctional Metal Ion Homeostasis and Xenobiotic Metal Exposure: Redox Signaling and Oxidative Stress. Antioxid Redox Signal 28, 1669-1703. https://doi.org/10.1089/ars.2017.7272.
13. Gui D, Cui Z, Zhang L, Yu C, Yao D, Xu M, et al., 2017. Salidroside attenuates hypoxia-induced pulmonary arterial smooth muscle cell proliferation and apoptosis resistance by upregulating autophagy through the AMPK-mTOR-ULK1 pathway. BMC Pulm Med 17, 191. https://doi.org/10.1186/s12890-017-0477-4.
14. Gupta R, Ambasta RK, Pravir K, 2021. Autophagy and apoptosis cascade: which is more prominent in neuronal death? Cell Mol Life Sci 78, 8001-8047. https://doi.org/10.1007/s00018-021-04004-4.
15. Herzig S, Shaw RJ, 2018. AMPK: guardian of metabolism and mitochondrial homeostasis. Nat Rev Mol Cell Biol 19, 121-135. https://doi.org/10.1038/nrm.2017.95.
16. Kaur I, Behl T, Aleya L, Rahman MH, Kumar A, Arora S, et al., 2021. Role of metallic pollutants in neurodegeneration: effects of aluminum, lead, mercury, and arsenic in mediating brain impairment

events and autism spectrum disorder. Environ Sci Pollut Res Int 28, 8989-9001. https://doi.org/10.1007/s11356-020-12255-0.

17. Klionsky DJ, Petroni G, Amaravadi RK, Baehrecke EH, Ballabio A, Boya P, et al., 2021. Autophagy in major human diseases. EMBO J 40, e108863. https://doi.org/10.15252/embj.2021108863.
18. Lange M, Joly F, Vardy J, Ahles T, Dubois M, Tron L, et al., 2019. Cancer-related cognitive impairment: an update on state of the art, detection, and management strategies in cancer survivors. Ann Oncol 30, 1925-1940. https://doi.org/10.1093/annonc/mdz410.
19. Li Y, Chen Y, 2019. AMPK and Autophagy. Adv Exp Med Biol 1206, 85-108. https://doi.org/10.1007/978-981-15-0602-4_4.
20. Liang MZ, Ke TL, Chen L, 2021. Mitochondrial Protein PGAM5 Emerges as a New Regulator in Neurological Diseases. Front Mol Neurosci 14, 730604. https://doi.org/10.3389/fnmol.2021.730604.
21. Liu J, Liu W, Yang H, 2019. Balancing Apoptosis and Autophagy for Parkinson's Disease Therapy: Targeting BCL-2. ACS Chem Neurosci 10, 792-802. https://doi.org/10.1021/acschemneuro.8b00356.
22. Liu J, Wei LX, Wang Q, Lu YF, Zhang F, Shi JZ, et al., 2018. A review of cinnabar (HgS) and/or realgar (As (4)S(4))-containing traditional medicines. J Ethnopharmacol 210, 340-350. https://doi.org/10.1016/j.jep.2017.08.037.
23. Luo Q, Song Y, Kang J, Wu Y, Wu F, Li Y, et al., 2021. mtROS-mediated Akt/AMPK/mTOR pathway was involved in Copper-induced autophagy and it attenuates Copper-induced apoptosis in RAW264.7 mouse monocytes. Redox Biol 41, 101912. https://doi.org/10.1016/j.redox.2021.101912.
24. Ma K, Zhang Z, Chang R, Cheng H, Mu C, Zhao T, et al., 2020. Dynamic PGAM5 multimers dephosphorylate BCL-xL or FUNDC1 to regulate mitochondrial and cellular fate. Cell Death Differ 27, 1036-1051. https://doi.org/10.1038/s41418-019-0396-4.
25. Nurchi VM, Djordjevic AB, Crisponi G, Alexander J, Bjorklund G, Aaseth J, 2020. Arsenic Toxicity: Molecular Targets and Therapeutic Agents. Biomolecules 10. https://doi.org/10.3390/biom10020235.
26. Prakash C, Chhikara S, Kumar V, 2022. Mitochondrial Dysfunction in Arsenic-Induced Hepatotoxicity: Pathogenic and Therapeutic Implications. Biol Trace Elem Res 200, 261-270. https://doi.org/10.1007/s12011-021-02624-2.
27. Qu N, Qu J, Huang N, Zhang K, Ye T, Shi J, et al., 2022. Calycosin induces autophagy and apoptosis via Sestrin2/AMPK/mTOR in human papillary thyroid cancer cells. Front Pharmacol 13, 1056687. https://doi.org/10.3389/fphar.2022.1056687.
28. Sekeres MJ, Bradley-Garcia M, Martinez-Canabal A, Winocur G, 2021. Chemotherapy-Induced Cognitive Impairment and Hippocampal Neurogenesis: A Review of Physiological Mechanisms and Interventions. Int J Mol Sci 22. https://doi.org/10.3390/ijms222312697.
29. Sekeres MJ, Winocur G, Moscovitch M, 2018. The hippocampus and related neocortical structures in memory transformation. Neurosci Lett 680, 39-53. https://doi.org/10.1016/j.neulet.2018.05.006.
30. Silva-Adaya D, Ramos-Chavez LA, Petrosyan P, Gonzalez-Alfonso WL, Perez-Acosta A, Gonsebatt ME, 2020. Early Neurotoxic Effects of Inorganic Arsenic Modulate Cortical GSH Levels Associated With

the Activation of the Nrf2 and NFkappaB Pathways, Expression of Amino Acid Transporters and NMDA Receptors and the Production of Hydrogen Sulfide. Front Cell Neurosci 14, 17. https://doi.org/10.3389/fncel.2020.00017.

31. Su Z, Yang Z, Xu Y, Chen Y, Yu Q, 2015. Apoptosis, autophagy, necroptosis, and cancer metastasis. Mol Cancer 14, 48. https://doi.org/10.1186/s12943-015-0321-5.
32. Takeda K, Komuro Y, Hayakawa T, Oguchi H, Ishida Y, Murakami S, et al., 2009. Mitochondrial phosphoglycerate mutase 5 uses alternate catalytic activity as a protein serine/threonine phosphatase to activate ASK1. Proc Natl Acad Sci U S A 106, 12301-5. https://doi.org/10.1073/pnas.0901823106.
33. Tschan MP, Simon HU, 2010. The role of autophagy in anticancer therapy: promises and uncertainties. J Intern Med 268, 410-8. https://doi.org/10.1111/j.1365-2796.2010.02266.x.
34. Wadgaonkar P, Chen F, 2021. Connections between endoplasmic reticulum stress-associated unfolded protein response, mitochondria, and autophagy in arsenic-induced carcinogenesis. Semin Cancer Biol 76, 258-266. https://doi.org/10.1016/j.semcancer.2021.04.004.
35. Wang K, 2015. Autophagy and apoptosis in liver injury. Cell Cycle 14, 1631-42. https://doi.org/10.1080/15384101.2015.1038685.
36. Wen YD, Sheng R, Zhang LS, Han R, Zhang X, Zhang XD, et al., 2008. Neuronal injury in rat model of permanent focal cerebral ischemia is associated with activation of autophagic and lysosomal pathways. Autophagy 4, 762-9. https://doi.org/10.4161/auto.6412.
37. Wu S, Zou MH, 2020. AMPK, Mitochondrial Function, and Cardiovascular Disease. Int J Mol Sci 21. https://doi.org/10.3390/ijms21144987.
38. Wu W, Tian W, Hu Z, Chen G, Huang L, Li W, et al., 2014. ULK1 translocates to mitochondria and phosphorylates FUNDC1 to regulate mitophagy. EMBO Rep 15, 566-75. https://doi.org/10.1002/embr.201438501.
39. Xin XY, Pan J, Wang XQ, Ma JF, Ding JQ, Yang GY, et al., 2011. 2-methoxyestradiol attenuates autophagy activation after global ischemia. Can J Neurol Sci 38, 631-8. https://doi.org/10.1017/s031716710001218x.
40. Zhang X, Mei D, Li Y, You M, Wang D, Yao D, et al., 2022. Arsenic exposure via drinking water during pregnancy and lactation induces autism-like behaviors in male offspring mice. Chemosphere 290, 133338. https://doi.org/10.1016/j.chemosphere.2021.133338.

Figures

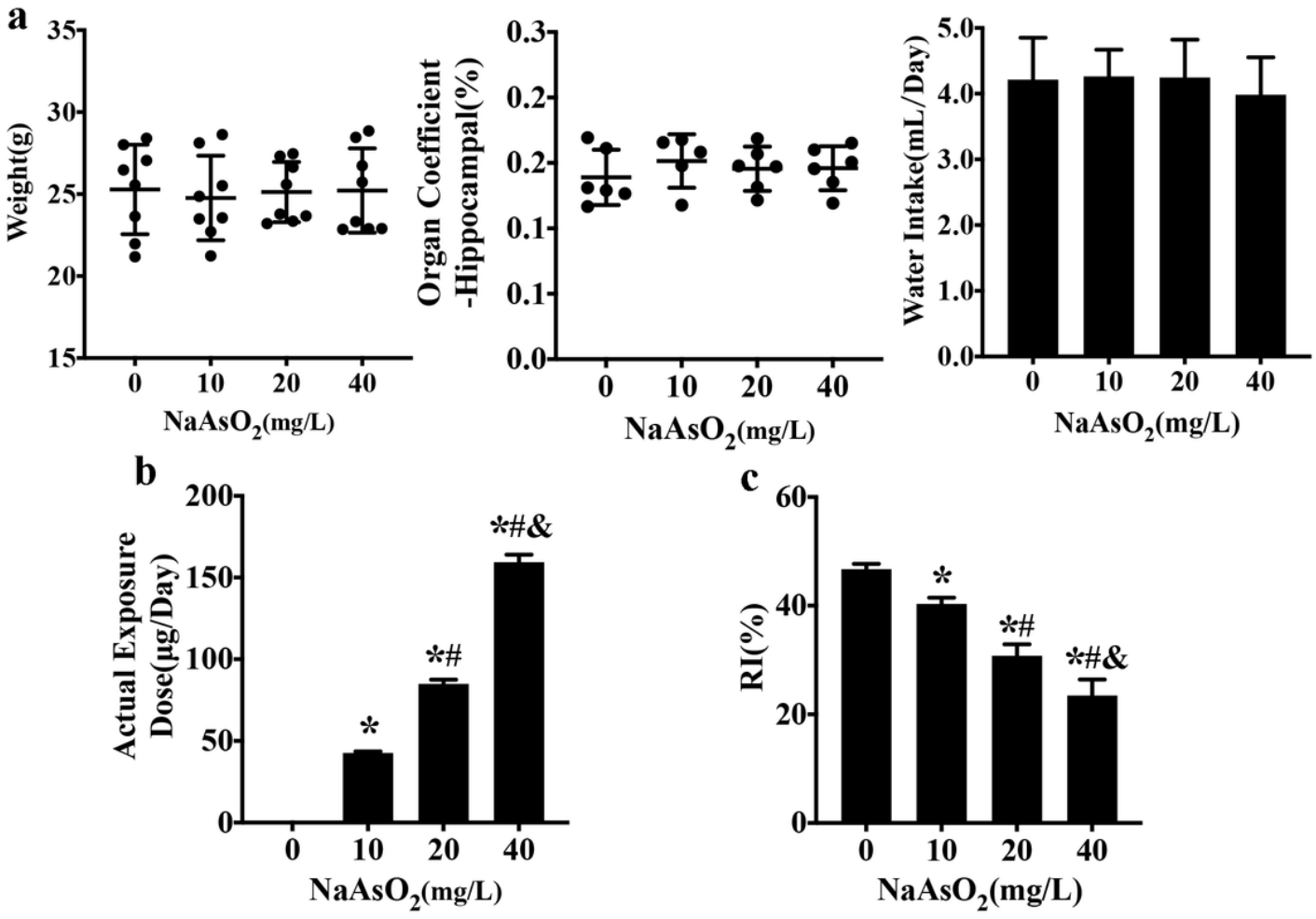

Figure 1

Normal condition and cognition damage of arsenic-exposed C57BL/6 mice. (a) Analysis of body weight, hippocampal organ coefficient and water intake of mice exposed to different doses of arsenic; (b) Actual daily arsenic exposure dose of mice; (c) Cognitive coefficient analysis of novel object recognition experiment. The RI of arsenic-exposed mice decreased significantly compared with that of the control group; *, vs. 0 mg/L group; #, vs. 10 mg/L group; &, vs. 20 mg/L group; n = 6.

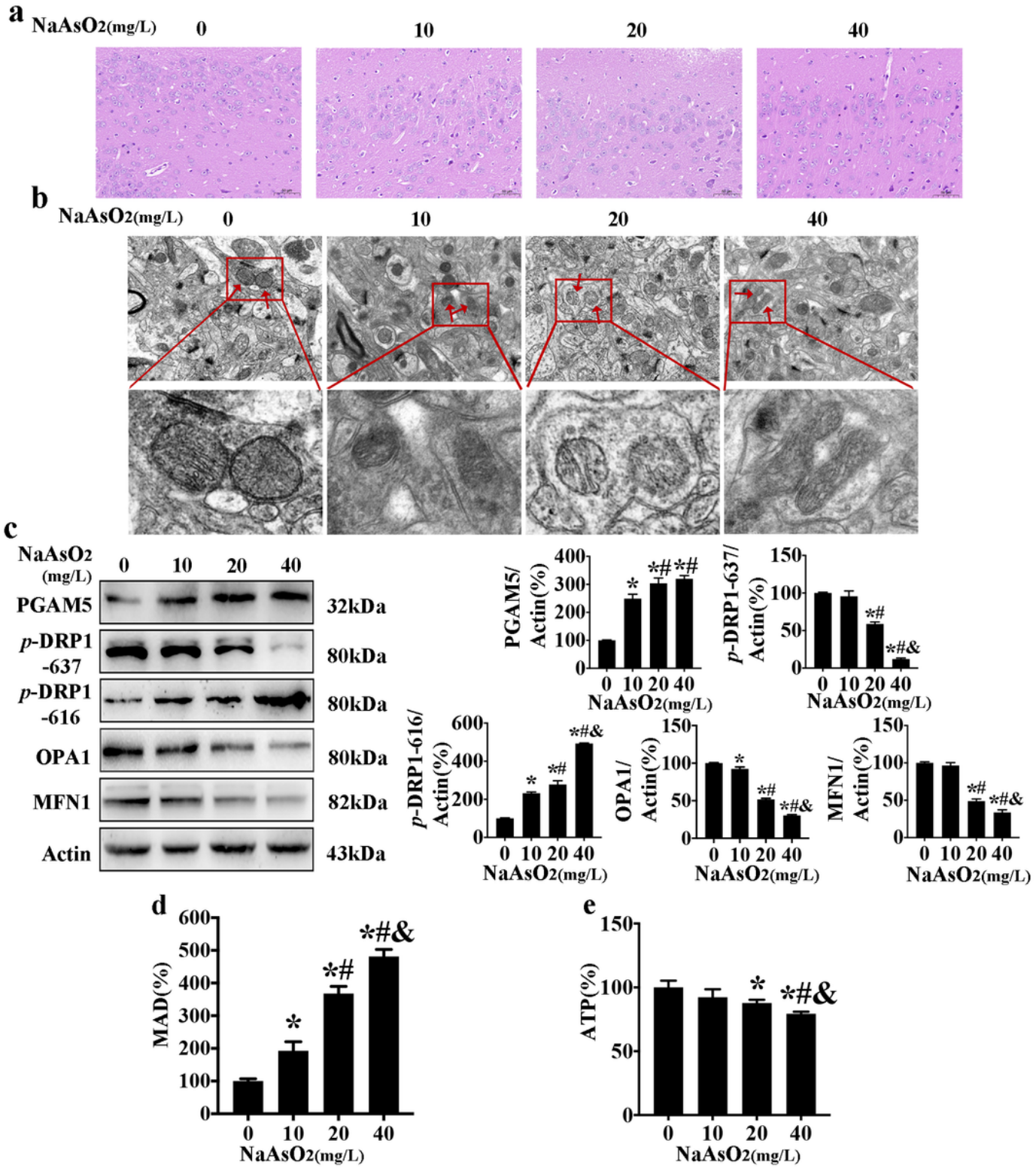

Figure 2

Mitochondria lesions in hippocampal neurons of chronic arsenic-exposed mice. (a) Results of H&E staining showed that along with the increase of arsenic concentration, the cell arrangement in the hippocampus of mice was gradually loosened and disordered; (b) Transmission electron microscopy demonstrated that the lesions to the integrity of mitochondrial bilayer membrane and the appearance of abnormal crest structure in hippocampal neurons aggravated along with the increase of arsenic exposure

level; (c) Chronic arsenic exposure affected levels of mitochondrial dynamic proteins in hippocampal neurons, including up-regulation of PGAM5 and *p*-DRP1 Ser616, and down-regulations of *p*-DRP1 Ser637, OPA1 and MFN1; (d) Dose-dependent increase of MDA was observed in arsenic-exposed mice hippocampus; (e) Decreased production of ATP in arsenic-exposed mice hippocampus; *, vs. 0 mg/L group; #, vs. 10 mg/L group; &, vs. 20 mg/L group; n = 6.

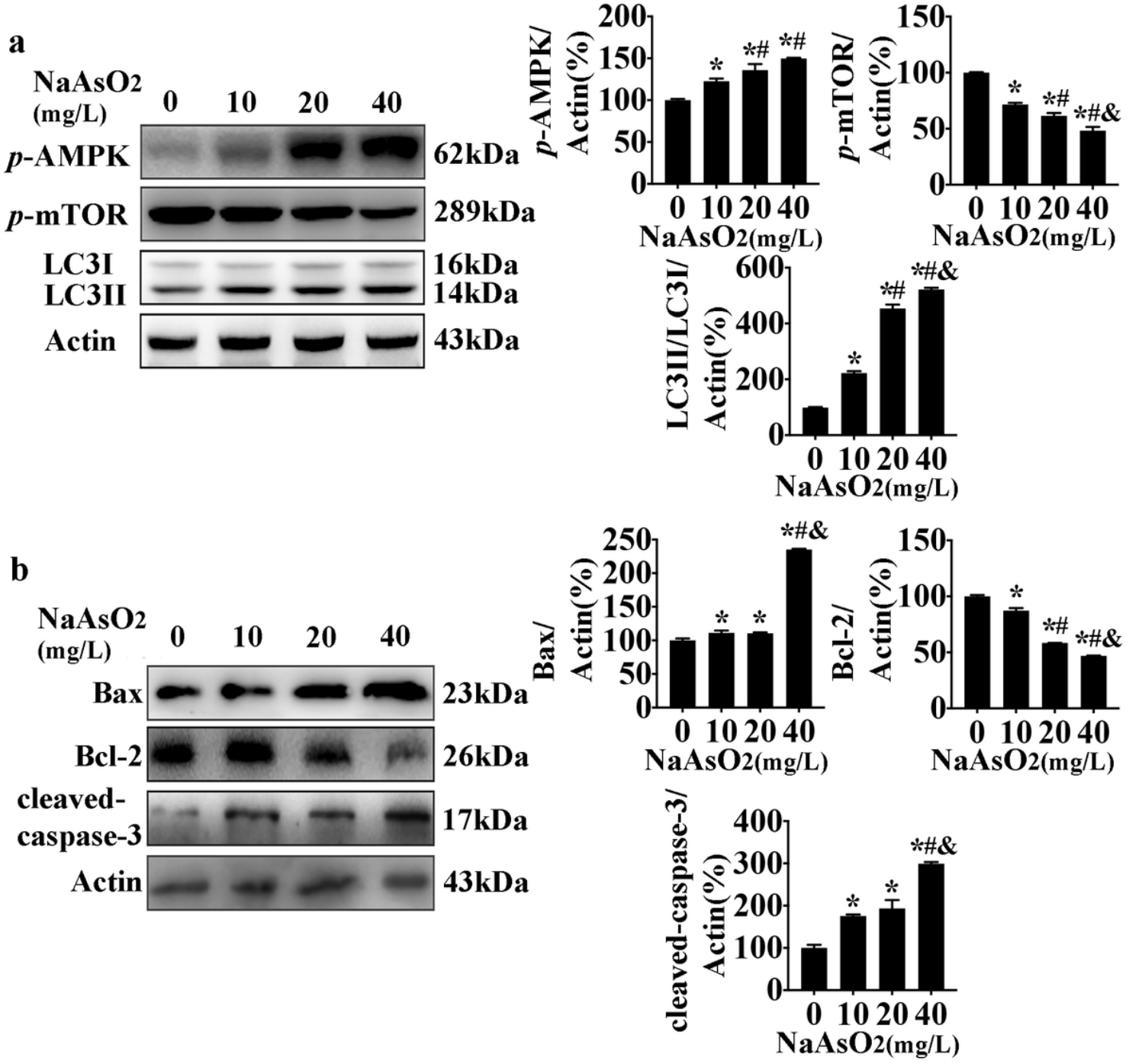

Figure 3

Apoptosis and AMPK-mTOR dependent autophagy were activated in hippocampal neurons of chronic arsenic-exposed mice. (a) Chronic arsenic exposure activated autophagy in hippocampal neurons, which

was demonstrated by dose-dependent up-regulation of *p*-AMPK and LC3, and down-regulation of *p*-mTOR; (b) Chronic arsenic exposure activated apoptosis in hippocampal neurons, which was demonstrated by increased Bax and cleaved-caspase-3, and decreased Bcl-2; *, vs. 0 mg/L group; #, vs. 10 mg/L group; &, vs. 20 mg/L group; n = 6.

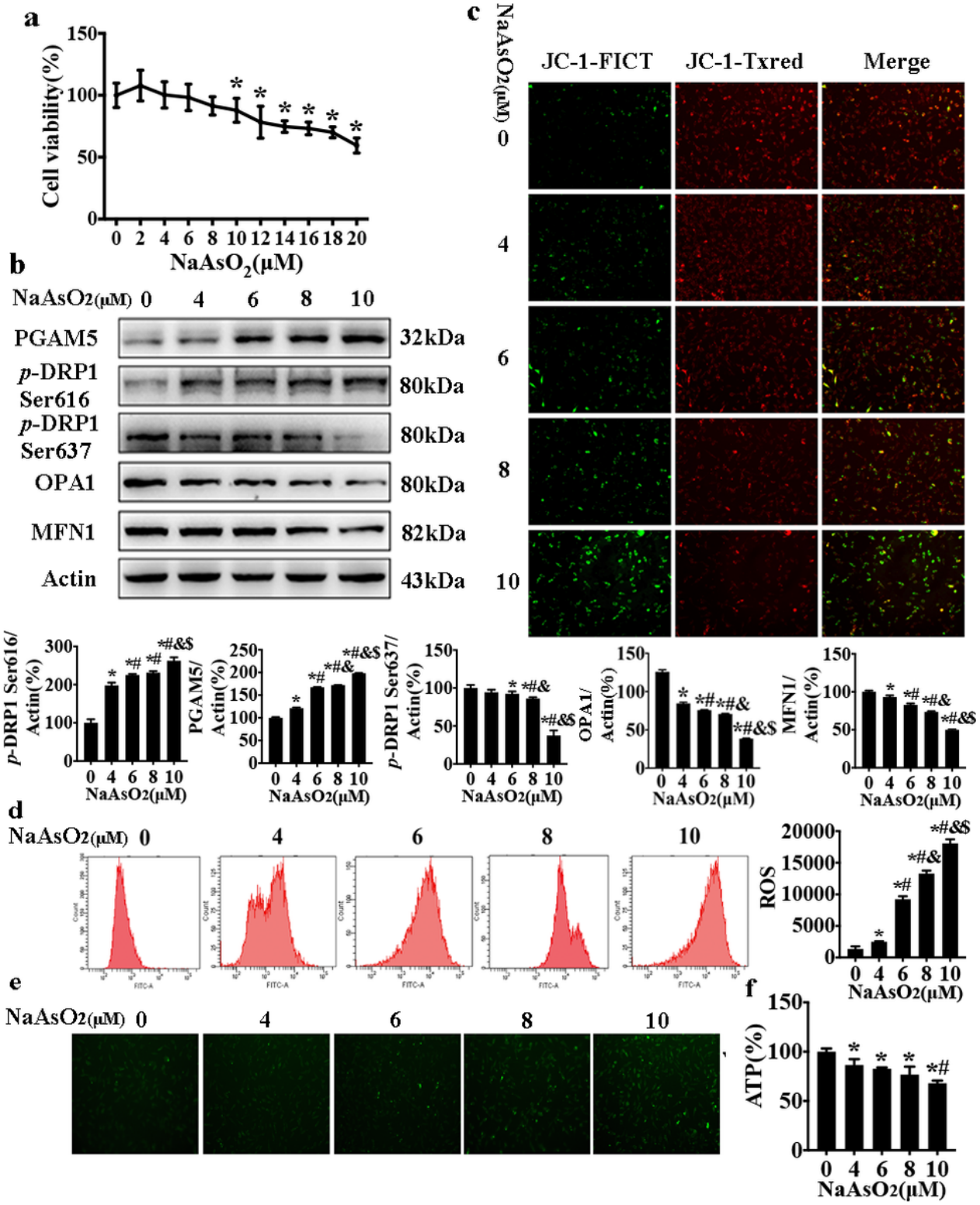

Figure 4

Mitochondria lesions in arsenic-exposed HT-22 cells. The mouse hippocampal neuron (HT-22) cells were treated with $NaAsO_2$ for 24 h. (a) Cell viability was significantly decreased when the concentration of $NaAsO_2$ was beyond 10 μM; (b) The dose-dependently significant down-regulation of *p*-DRP1 Ser637, OPA1 and MFN1, and up-regulation of PGAM5 and *p*-DRP1 Ser616 were revealed by western blot assay; (c) The fluorescence intensity of $NaAsO_2$-exposed cells stained by Txred faded gradually, while the fluorescence intensity stained by FICT enhanced gradually; (d) $NaAsO_2$-induced dose-dependently increased ROS was illustrated by flow cytometry; (e) An increased tendency of ROS fluorescence intensity in $NaAsO_2$-exposed cells was illustrated by dichlorofluorescein fluorescence staining; (f) The significantly decreased ATP levels in $NaAsO_2$-exposed cells was illustrated by ATP analysis; *, vs. 0 μM group; #, vs. 4 μM group; &, vs. 6 μM group; $, vs. 8 μM group; n = 3.

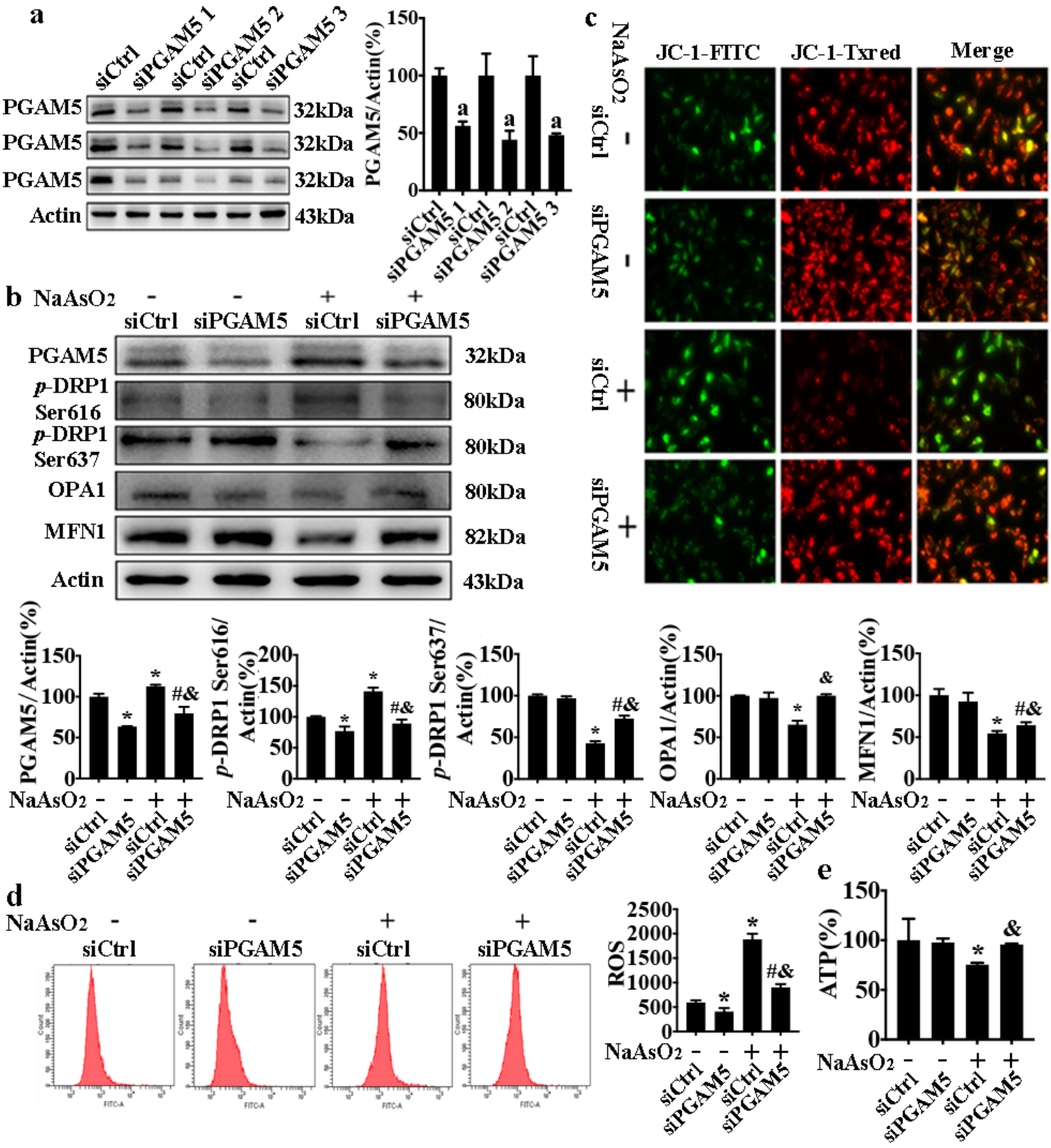

Figure 5

PGAM5 played a role in arsenic-induced mitochondrial lesions due to mitochondrial dynamic disorder. HT-22 cells were treated by siPGAM5 (50 nM) and $NaAsO_2$ at the concentration of 10 μM for 24 h. (a) Similar silencing effects were obtained from 3 siRNA oligonucleotides targeting at PGAM5; (b) Intervention by siPGAM5 significantly attenuated the levels of PGAM5 and *p*-DRP1 Ser616, while enhanced the levels of *p*-DRP1 Ser637, OPA1 and MFN1; (c) Intervention by siPGAM5 enhanced red fluorescence intensity

stained by Txred but decreased green fluorescence intensity stained by FICT, indicating the recovery of mitochondrial membrane potential; (d) Compared with the arsenic-exposed group, ROS level in siPGAM5-treated group significantly decreased; (e) Arsenic-induced ATP depletion was recovered in siPGAM5-treated cells; a, vs. siCtrl; *, vs. $NaAsO_2$ (-)/siCtrl group; #, vs. $NaAsO_2$ (-)/siPGAM5 group; &, vs. $NaAsO_2$ (+)/siCtrl group; n = 3.

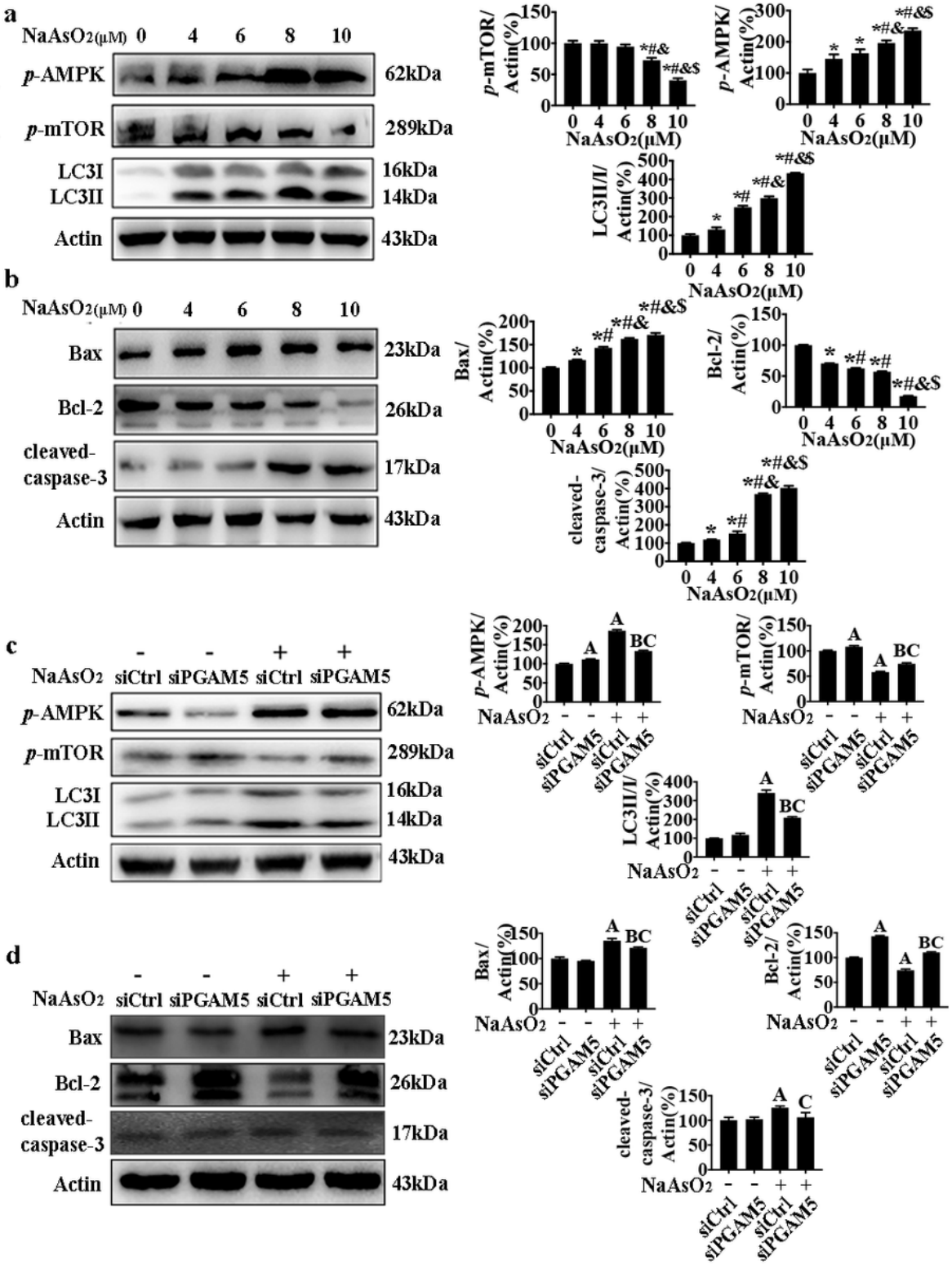

Figure 6

Activation of AMPK-mTOR dependent autophagy and apoptosis in arsenic-exposed HT-22 cells. It was partially reversed by siPGAM5. Cells were treated with siPGAM5 (50 nM) and $NaAsO_2$ at the concentration of 10 μM for 24 h. (a) $NaAsO_2$-induced autophagy was demonstrated by the significant up-regulation of *p*-AMPK and LC3, and down-regulation of *p*-mTOR; (b) $NaAsO_2$-induced apoptosis was demonstrated by the significant increase of Bax and cleaved-caspase-3, and decrease of Bcl-2 by western blot assay; (c) Compared with the control group, significantly decreased levels of *p*-AMPK and LC3, and increased level of *p*-mTOR were found in the siPGAM5 intervention group; (d) Significantly decreased levels of Bax and cleaved-caspase-3, and increased level of Bcl-2 were observed in the group of siPGAM5 intervention; *, vs. 0 μM group; #, vs. 4 μM group; &, vs. 6 μM group; $, vs. 8 μM group; A, vs. $NaAsO_2$ (-)/siCtrl group; B, vs. $NaAsO_2$ (-)/siPGAM5 group; C, vs. $NaAsO_2$ (+)/siCtrl group; n = 3.

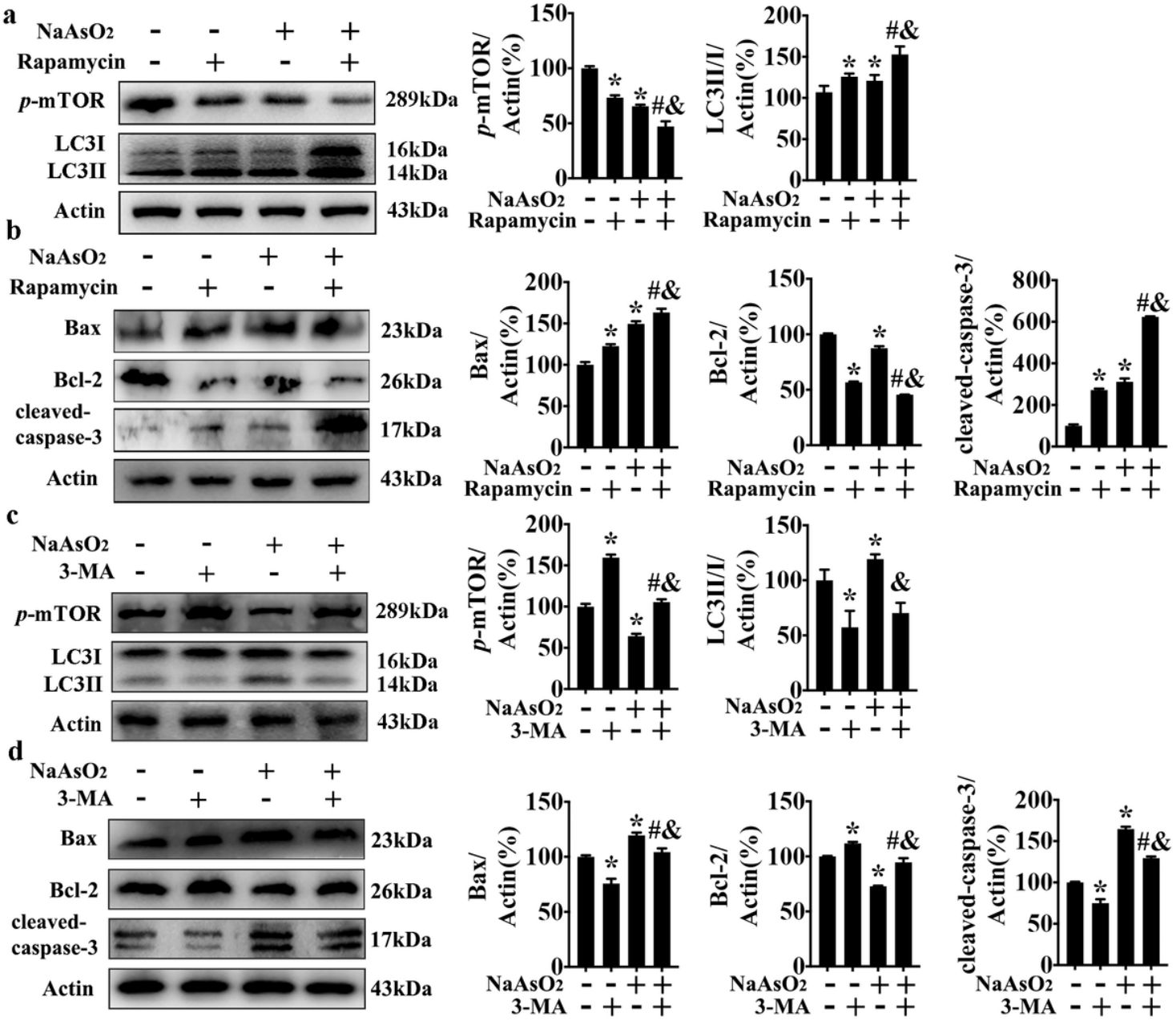

Figure 7

Autophagy regulated apoptosis in HT-22 cells. Cells were treated with rapamycin (2 nM) or 3-MA (5 mM) for 1 hour prior to $NaAsO_2$ exposure (10 μM, 24 h). (a) Compared with the control cells, rapamycin-treated cells demonstrated significant down-regulation of *p*-mTOR but up-regulation of LC3; (b) Compared with the control cells, rapamycin-treated cells showed prominent up-regulations of Bax and cleaved-caspase-3, but down-regulation of Bcl-2; (c) Compared with the control cells, 3-MA-treated cells demonstrated significant down-regulation of LC3, but up-regulation of *p*-mTOR; (d) Compared with the control cells, 3-MA-treated cells showed significant down-regulations of Bax and cleaved-caspase-3, but up-regulation of Bcl-2; *, vs. $NaAsO_2$ (-)/3-MA or rapamycin (-) group; #, vs. $NaAsO_2$ (-)/3-MA or rapamycin (+) group; &, vs. $NaAsO_2$ (+)/3-MA or rapamycin (-) group; n = 3.

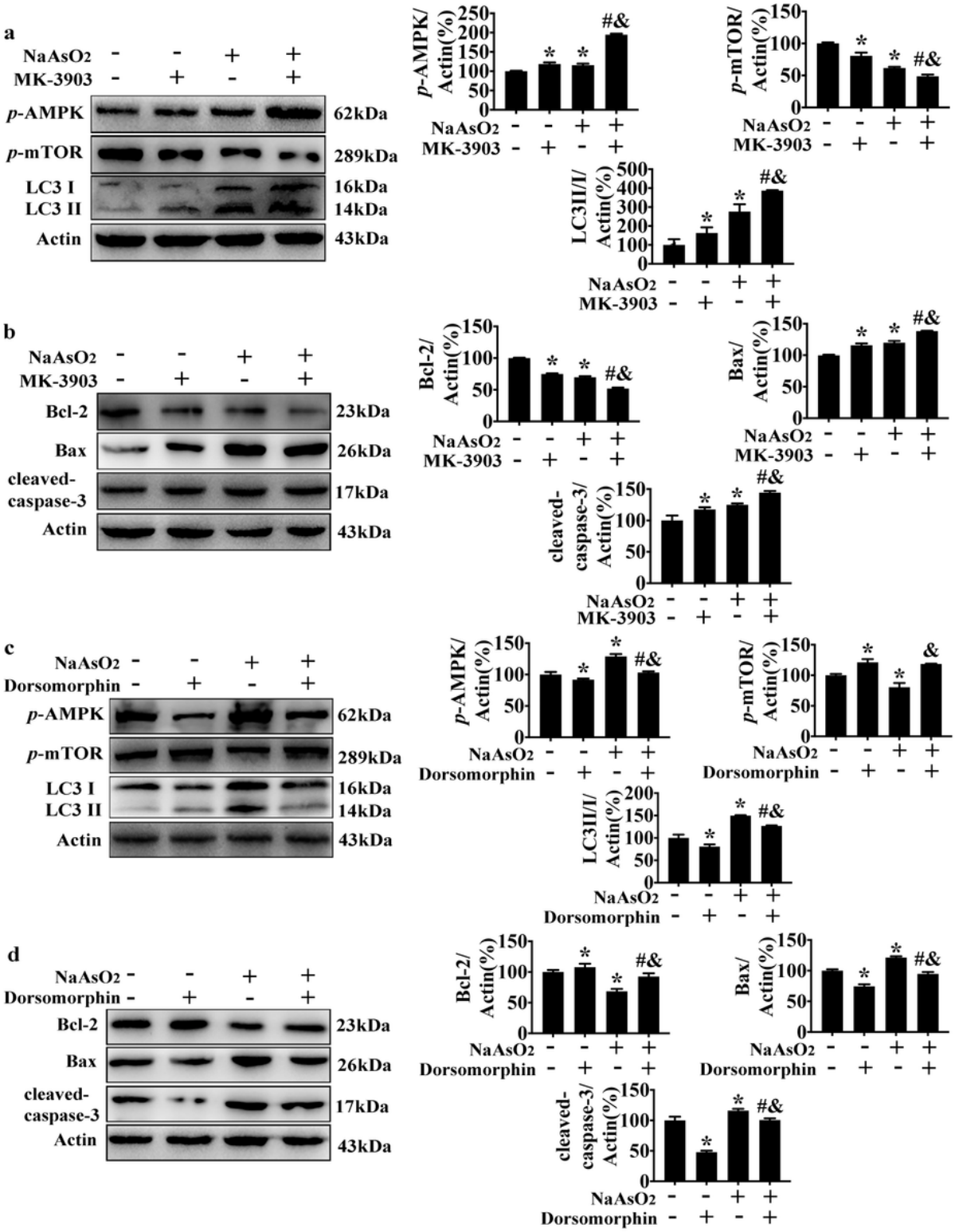

Figure 8

Arsenic-induced autophagy and apoptosis activation was partially reversed by MK-3903 or dorsomorphin in HT-22 cells. Cells were pre-treated with MK-3903 (4 nM) or dorsomorphin (5 μM) for 1 h, followed by exposure to $NaAsO_2$ at the concentration of 10 μM for 24 h. (a) Compared with the arsenic-exposed group, significantly increased levels of *p*-AMPK and LC3, and decreased level of *p*-mTOR were found in the MK-3903 intervention group; (b) Compared with the arsenic-exposed group, significantly decreased

levels of Bcl-2, and increased level of Bax and cleaved-caspase-3 were found in the MK-3903 intervention group; (c) Significantly increased levels of *p*-mTOR, and decreased level of *p*-AMPK and LC3 were observed in the group of dorsomorphin intervention; (d) Significantly increased levels of Bcl-2, and decreased level of Bax and cleaved-caspase-3 were observed in the group of dorsomorphin intervention; *, vs. $NaAsO_2$ (-)/MK-3903 or dorsomorphin (-) group; #, vs. $NaAsO_2$ (-)/MK-3903 or dorsomorphin (+) group; &, vs. $NaAsO_2$ (+)/MK-3903 or dorsomorphin (+) group; n = 3.